Numerical study of Silicon Heterojunction Solar Cells with nc-SiC/SiO_2 Based Transparent Passivating Contact

Habtamu T. Gebrewold[1,2], Karsten Bittkau[1], Kaifu Qiu[1] and Kaining Ding[1]

[1] IEK5 – Photovoltaik, Forschungszentrum Jülich GmbH, 52425 Jülich, Germany

[2] Faculty of Electrical Engineering and Information Technology, RWTH Aachen University, 52074 Aachen, Germany

***Abstract*—Silicon heterojunction with nc-SiC(n)/SiO_2 based front transparent passivating contact (TPC) is numerically modeled. The model is then used to study the effect of active dopant concentration at the front and rear contact of the solar cell. A potential of power conversion efficiency above 25 % can be achieved with a suitable acceptor dopant concentration of p-type amorphous silicon at the rear side. Improving fill factor via SiC dopant concentration can enhance the cell power conversion efficiency within a narrow range of active dopant concentration. However, very high doping of SiC can affect the cell performance negatively.**

Keywords—Silicon heterojunction solar cell, transparent passivating contact, Numerical simulation, Tunneling

I. INTRODUCTION

Silicon heterojunction (SHJ) solar cells have received much attention in recent years. Hydrogenated amorphous silicon (a-Si:H) based SHJ is known to have excellent surface passivation, hence, improved open-circuit voltage (V_{oc}) and power conversion efficiency (η). However, the a-Si:H layers and transparent conductive oxide (TCO) layer introduce parasitic absorption loss, especially at the front side. Hydrogenated amorphous silicon strongly absorbs light in the short wavelength range. Reducing this parasitic absorption will improve short circuit current density (J_{sc}); thus, it will improve the solar cell's power conversion efficiency. One of the solutions to avoid parasitic absorption at the front side is using interdigitated back contact (IBC) architecture. In this architecture, the contact layers are exclusively at the back side, no front contact is present. So, the associated parasitic absorptions will be reduced. In addition to the parasitic absorption in the front layers, IBC architecture avoids shading loss due to front metallization. However, IBC architecture involves too many processes and fabrication steps that are too expensive for large-scale production.

Another way to reduce parasitic absorption at the front side is to find alternative better materials with a wider bandgap. Wide bandgap materials are transparent for a significant portion of the solar spectrum and have low absorption coefficient, therefore, show less parasitic absorption. However, it should be not only transparent but also provide good passivation and conduction. A stack of hydrogenated nanocrystalline silicon carbide (nc-SiC:H), a suitable alternative wide bandgap material, and a few nano-meter tunnel oxide (SiO_2) layer has been reported to provide both transparency and passivation [1, 2]. Hence, it is called transparent passivating contact (TPC). A solar cell with TPC front and amorphous silicon-based heterojunction at the rear side has been developed and investigated at our institute. This so-called TPC silicon solar cell has improved J_{sc} and η. A 23.99 % certified efficiency and J_{sc} = 40.9 mA/cm^2 have been achieved so far. Further improvements need further study and understanding. Numerical modeling is vital in this regard.

In this work, we modeled a silicon solar cell with transparent passivating contact at the front side and a-Si:H -based heterojunction rear contact (TPC-SHJ solar cell), see Fig. 1. Our simulation model showed an excellent agreement to the measurement. The simulation model is then used to assess the potential for further improvement of the TPC-SHJ solar cell.

II. NUMERICAL MODEL

A. Simulation approach and parameters

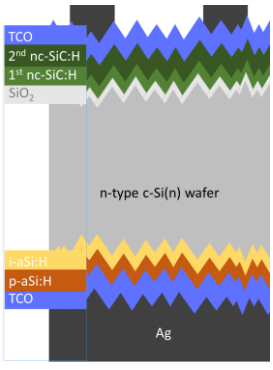

Fig. 1. The cross-sectional view of crystalline silicon solar cell with transparent passivating contact (TPC) layers stack at the front side and a-Si:H based silicon heterojunction at the rear side that is used in this work. The TPC stack consists of SiO_2 (tunnel oxide), 1st nc-SiC:H (low doped passivating layer), 2nd nc-SiC:H (highly doped conducting layer).

The cross-section of the modeled solar cell in this work is shown in Fig. 1. The rear side layout includes full metallization,

a sputtered indium tin oxide (100 nm), p-type (5 nm) and intrinsic (5 nm) a-Si:H. At the front side, a TPC stack consisting of wet-chemically grown SiO_2 (~1.4 nm), a double layer of (2.5 nm and 30 nm) nanocrystalline silicon carbide nc-SiC:H(n) and indium tin oxide (70 nm). The simulation is conducted with Sentaurus TCAD [3].

A summary of important input parameters used for the model is given in Table I and Table II. Most of the general input parameters concerning the semiconductor properties of crystalline and amorphous silicon are used as in [4] and can be found elsewhere.

TABLE I. IMPORTANT SIMULATION PARAMETERS OF C-SI

c-Si	
Parameters	
Auger and radiative recombination	Richter et al. [5], Nguyen et al. [6]
Intrinsic carrier density	P. Altermatt et al. [7] (9.65·109 cm−3 at T =300 K)
Wafer resistivity	1.0 Ωcm, n-type

For nc-SiC:H layers, material properties of 3C-SiC as in [8] and parameters measured experimentally in our institute as in TABLE II were used. Material parameters of sputtered ITO according to measurement or otherwise as in [4] are shown in TABLE II.

TABLE II. IMPORTANT SIMULATION PARAMETERS OF SIC AND ITO

SiC		
Parameters	***Passiv. SiC***	***Cond. SiC***
Active doping concentaration (cm^{-3})	$2.0x10^{20}$	$7.0x10^{20}$
Band gap (eV)	2.7	3.0
Electron affinity (eV)	2.93	2.93
ITO		
Parameters	***Front***	***Rear***
Active carrier concentaration (cm^{-3})	$1.68x10^{20}$	$1.4x10^{20}$
Mobility (cm^2/Vs)	27.6	22.0
Bandgap (eV)	3.7	3.7
Electron affinity (eV)	4.9	4.9

Carrier transport through tunneling thin oxide layer is modeled using non-local tunneling model as implemented in Sentaurus TCAD [3]. For carrier transport at the rear side, both band-to-band tunneling, as implemented in Sentaurus TCAD, and trap-assisted tunneling through traps in amorphous layers is considered. Tunneling effective masses used for the oxide barrier are $0.7*m_0$ and $0.32*m_0$ for elecctrons and holes, respectively; and, $0.1*m_0$ for amorphous silicon at the rear side [9]. m_0 is the rest mass of an electron.

An input optical generation profile is calculated using a 3D optical simulation result of total absorption in each modeled solar cell layers. The 3D optical simulation result agrees very well with the experimentally measured external quantum efficiency. The lamped parameter, i.e. total optical absorption, is used to determine the 2D optical generation profile as in [10]. The resulting 2D optical generation profile is used as an input to the electrical device simulation.

B. Simulation result

The simulated current density vs. voltage (J(V)) curves compared to experimentally measured are shown in Fig. 2. Our simulation is in good agreement with the experimentally measured curves for the interface trap density of $1.0x10^{12}$ cm^{-2} eV^{-1} at the SiO_2/c-Si interface and $1.0x10^{9}$ $cm^{-2}eV^{-1}$ at c-Si/i-a-Si:H. These values are well in the range of reported values elsewhere for the respective type of interfaces. In addition to 1 sun of AM1.5g incident spectrum, we simulated current density vs. voltage, J(V), curves for different numbers of sun by varying the incident light intensity. Our model agreed well for a different number of suns, i.e., different photo-generated carrier injection levels. The J_{sc}-V_{oc} curve is also in good agreement with the experiment.

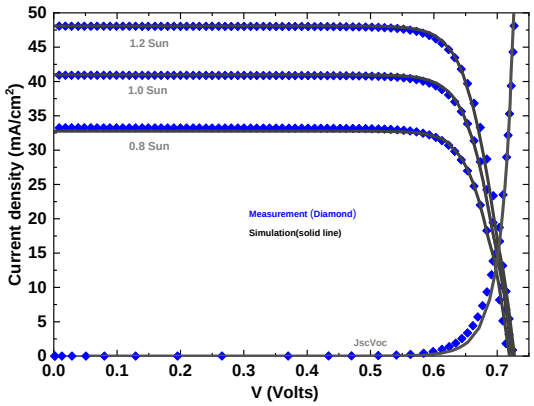

Fig. 2. Experiment vs simulation of crystalline silicon solar cell with transparent passivating contact (TPC) layers stack at the front side and a-Si:H based silicon hetrojunction at the rear side (TPC-SHJ solar cell). TPC-SHJ solar cell's J(V) for a different number of suns, and Jsc-Voc curve. Note that this result include MgF_2 antireflection layer on top of TPC-SHJ solar cell.

III. RESULT AND DISCUSSION

Using the simulation model presented in the previous section, we studied the role and impact of active dopant concentration in the conductive silicon carbide layer and the p-type amorphous silicon layer.

A. Hole transport contact

Here, we varied active dopant concentration, which is equivalent to the variation of activation energy. Keeping the ITO layer's carrier concentration to $N_{ITO} = 1.4x10^{20}$ cm^{-3}, we varied the active dopant concentration at the p-type amorphous silicon as shown in Fig. 3. The p-aSi:H layer activation energy plays an important role in achieving the required band bending and carrier transporting towards ITO through tunneling. For a fixed N_{ITO}, both fill factor (*FF*), the cell's V_{oc}, and conversion efficiency are improved as active dopant concentration increases. However, it saturates at a value which is high enough that the valence band of the p-aSi:H layer aligns very well with the conduction band of the ITO. In this case, carrier transport is mainly through band-to-band tunneling, i.e., holes from the

valence band of p-a-Si:H side and electrons from the conduction band of ITO side recombine via tunneling.

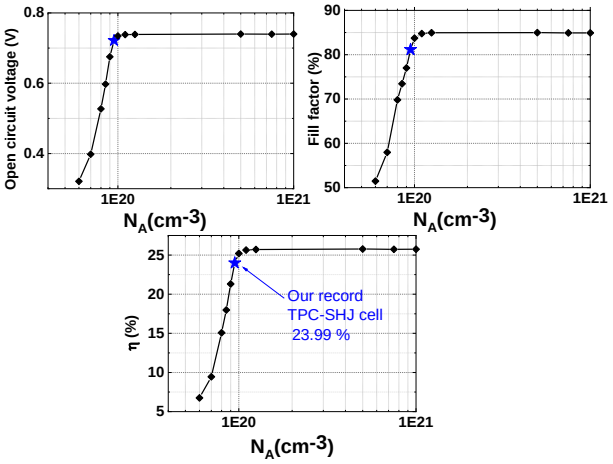

Fig. 3. Open circuit voltage, fill factor, and power conversion efficiency as a function of active dopant concentration of p-a-Si:H layer in TPC-SHJ solar cell.

From Fig. 3, it is apparent that a high fill factor, around 85 % for a realistic interface, can be achieved for a suitable active dopant concentration of p-a-Si:H. Similarly, a V_{oc} around 740 mV can be achieved for a realistic interface. As a result, TPC–SHJ cell can be optimized to get efficiency, potentially, above 25 % with a realistic defect density at the wafer interfaces. An optical optimization of the front contact without significantly changing the electrical properties can further improve the potential power conversion efficiency.

B. Electron transport contact

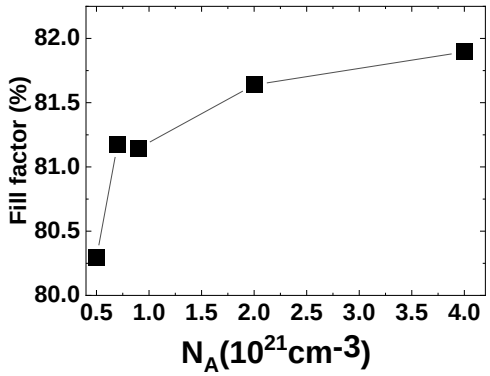

Fig. 4. Fill factor as a function of active dopant concentration of the 2nd nc-SiC:H (conductive nc-SiC:H) layer in TPC-SHJ solar cell.

In Fig. 4, we varied the active dopant concentration of the second nc-SiC:H layer, i.e., conductive SiC layer. It is vital for front side conductivity. As this layer gets more conductive with the carrier concentration, the resistive loss gets reduced. Hence, the fill factor of the solar cell is improved as a result. However, experimentally tuning active dopant concentration is not a trivial task because other aspects of the material can change unintended. These unintended changes may include optical absorption properties and a change in the crystalline structure of nc-SiC:H, resulting in the formation of different phases of SiC polytypes. Different polytypes of SiC have different semiconductor properties. Therefore, studying the effect of dopant concentration of nc-SiC:H over wide ranges need comprehensive modeling. Besides, the dopant concentration of nc-SiC:H could affect the ohmic contact properties of nc-SiC:H with ITO, nc-SiC:H/ITO contact.

IV. CONCLUSIONS

Silicon heterojunction with front transparent passivating contact (TPC) is numerically modeled. The model is then used to study the effect of active dopant concentration of p-a-Si:H and silicon carbide at the rear and front sides, respectively. A potential conversion efficiency above 25 % can be achieved with a suitable dopant concentration of p-a-Si:H. Improving fill factor via SiC dopant concentration can further improve the cell efficiency within a narrow range of active dopant concentration.

ACKNOWLEDGMENT

This work was supported by the Federal Ministry of Economic Affairs and Energy in the framework of the TUKAN project (grant: 0324198D) and the (HEMF) Helmholtz Energy Materials Foundry infrastructure funded by the HGF (Helmholtz association).

REFERENCES

[1] M. Pomaska et al., "Transparent silicon carbide/tunnel SiO 2 passivation for c ‐ Si solar cell front side: Enabling Jsc > 42 mA/cm 2 and i Voc of 742 mV," Prog Photovolt Res Appl, vol. 28, no. 4, pp. 321‐327, 2020

[2] M. Kohler et al., "Optimization of Transparent Passivating Contact for Crystalline Silicon Solar Cells," IEEE J. Photovoltaics, vol. 10, no. 1, pp. 46–53, 2020

[3] I. Synopsys, Sentaurus™ Device User Guide.

[4] P. Procel et al., "The role of heterointerfaces and subgap energy states on transport mechanisms in silicon heterojunction solar cells," Prog Photovolt Res Appl, vol. 28, no. 9, pp. 935–945, 2020

[5] A. Richter, S. W. Glunz, F. Werner, J. Schmidt, and A. Cuevas, "Improved quantitative description of Auger recombination in crystalline silicon," Phys. Rev. B, vol. 86, no. 16, p. 165202, 2012

[6] H. T. Nguyen, S. C. Baker-Finch, and D. Macdonald, "Temperature dependence of the radiative recombination coefficient in crystalline silicon from spectral photoluminescence," Appl. Phys. Lett., vol. 104, no. 11, p. 112105, 2014

[7] Pietro P. Altermatt, Andreas Schenk, Frank Geelhaar, and Gernot Heiser, "Reassessment of the intrinsic carrier density in crystalline silicon in view of band-gap narrowing," Journal of Applied Physics, vol. 93, no. 3, p. 1598, 2003.

[8] N. Lophitis, A. Arvanitopoulos, S. Perkins, and M. Antoniou, "TCAD Device Modelling and Simulation of Wide Bandgap Power Semiconductors," in Disruptive wide bandgap semiconductors, related technologies, and their applications, Y. K. Sharma, Ed., London: IntechOpen, 2018.

[9] J. M. Shannon and K. J. B. M. Nieuwesteeg, "Tunneling effective mass in hydrogenated amorphous silicon," Appl. Phys. Lett., vol. 62, no. 15, pp. 1815–1817

[10] A. Fell and K. R. McIntosh, "Determining the generation profile for silicon solar cells from lumped optical parameters," pp. 1–5.